Real-Time Management of Power Systems With V2G Facility for Smart-Grid Applications

Uwakwe Christian Chukwu, *Student Member, IEEE*, and Satish M. Mahajan, *Senior Member, IEEE*

***Abstract*—Real-time application in power systems *is* a key to smart-grid realization. Maintaining accurate security information and monitoring the changing system state are necessary for real-time management of the modern-day power system. Smart-grid applications provide an excellent opportunity to better manage the voltage stability of the power system. Using intelligent electronic devices, it is possible to capture power system data, and give an instantaneous snapshot of the system status. The penetration of vehicle-to-grid (V2G) into the power system may introduce a high-level of volatility due precarious charging/discharging operations, hence emphasizing the need for a real-time management option. In this paper, a real-time monitoring diagnostic of the power system is presented. The system parameters for consideration are voltage profile, voltage stability, step voltage regulators (SVRs) operations, power, and energy loss. Economic studies are also considered. Results show that for a given V2G penetration level, three-phase and system-wide V2G integration results in an improved system performance, and economic operation of the power system than a one-phase V2G integration. Results also indicate that using V2G parking lots to inject reactive power to the grid at an optimal location can promise about 95% power/energy loss reduction (relative to power loss without V2G installed). The results are suitable for further applications of smart grids.**

***Index Terms*—Distribution system, economics, energy/power loss, Radial Distribution Analysis Package (RDAP), step voltage regulator (SVR), vehicle-to-grid (V2G), voltage profile, voltage stability.**

I. Introduction

REAL-TIME management of the electric power systems is very crucial in order to improve the efficiency, reliability, economics, and sustainability of electricity services. This step is being taken at this time to cooperate with various smart-grid and grid modernization efforts for a resilient system operation. Vehicle-to-grid (V2G) is a key component of the smart-grid initiative. However, the penetration of V2G into the distribution network may cause a high level of volatility and undesirable performance if real-time system monitoring is not considered. Ensuring secure operation of the power system requires both careful planning and operational strategies, since safe and economic operation cannot be compromised. However, the restructuring of the power system industry has heightened the need for more rigorous security assessment. An earlier study indicated that distributed energy sources (including V2G) can potentially affect the performance (and quality of service) of the power system [1]. V2G may threaten the system security, based on the following considerations: 1) increased uncertainty in day-to-day system operations; and 2) increased potential sources for system disturbances. Moreover, uncontrolled and random V2G charging can cause increased power/energy losses, overloads, interarea oscillations, increased exposure to voltage instability, and voltage fluctuations [2]. Hence, it has become insufficient, if not impossible, to operate the power systems with an acceptable degree of security by using the traditional operational planning studies that are conducted offline. The catastrophic North American blackout on August 14th 2003 highlights the importance of effective real-time management of the power system [3]. Hence, the penetration of V2G into the power system requires a real-time management paradigm in order to support the critical operations in the event of dynamic load change (due to V2G charging) or real/reactive power injections (due to V2G discharging power to grid). The mismatch between generation and load, which leads to power imbalance, and consequently voltage and frequency fluctuations, can be alleviated by real-time management.

V2Gs have been pursued to meet the increasing power demand and environmental sustainability initiatives, in addition to several power system applications [4]–[6]. Applications of V2G for supporting renewable energy units and stabilizing the grid were investigated [7]. Its potential as a new source of power was studied in [8] and [9]. Recent studies show that V2G can be modularly organized as parking lots [10]. A technique for scheduling the V2G in a constrained parking lot has been proposed [11]. This work assumes V2G parking lots (VPLs) in the distribution network. No known previous work has been performed to investigate the real-time management of power systems with V2G facilities. An attempt is made to fill the void through this work. The proposed algorithmic procedure is aimed at developing a tool that would help improve system performance through real-time monitoring of the power system performance. This paper, therefore, presents an algorithmic procedure for real-time management of the power system for smart-grid applications.

This paper is organized as follows. In Section II, the model of a V2G parking lot is presented, while modeling of power system parameters for real-time monitoring is presented in Section III.

Manuscript received May 28, 2012; revised February 19, 2013; accepted June 23, 2013. This work was supported by the Office of Research and Graduate Studies, Tennessee Technological University, Cookeville, TN, USA.

U. C. Chukwu is with the Department of Industrial and Electrical Engineering Technology, South Carolina State University, Orangeburg, SC 29117 USA (e-mail: uchukwu@scsu.edu).

S. M. Mahajan is with the Electrical and Computer Engineering Department, Tennessee Technological University, Cookeville, TN 38505 USA (e-mail: smahajan@tntech.edu).

Color versions of one or more of the figures in this paper are available online at http://ieeexplore.ieee.org.

Digital Object Identifier 10.1109/TSTE.2013.2273314

The real-time management algorithm is presented in Section IV, and numerical results in Section V. Conclusions are presented in Section VI.

II. Modeling of V2G Parking Lot

Accurate modeling of a VPL is critical in the analysis of the distribution system. The V2G units are either charging or discharging their batteries. For n-VPL comprising of n_s V2G units supplying power to the grid, and n_d vehicles charging their batteries, the net power, P_{net}, to the grid is [4], [16]

$$P_{\text{net}} = \sum_{i=1}^{n_s} P_{\text{EVo}_i}\left(1 - e^{-\beta_i t_{s_i}/t_{\max}}\right) - P_{\max}\left(n_d - \sum_{i=1}^{n_d} e^{-\alpha_i t_{c_i}/t_{\max}}\right) \quad (1)$$

where α_i and β_i are, respectively, the battery charging and discharging constants for an ith V2G unit, requiring charging time t_{ci}, and discharging time t_{si}. The parameters $P_{\max}$ and P_{EVo}, respectively, represent the maximum battery capacity and initial power in the V2G battery. The parameters in (1) could be obtained in real-time, and posted to a solver for computation of the VPL net power capacity. In this paper, Radial Distribution Analysis Package (RDAP) was used to run power flow analysis so as to investigate the impact of V2G power injection or consumption on the electric network. It is a common practice to model current source buses as negative PQ (hence, V2G is modeled as such when injecting power) [1]. The results provided information on the voltage profile and power loss requirements of the network. The RDAP also provided information that is important for an economic analysis and voltage stability assessment of the system.

Power electronics and related control systems are required for the operation of VPL on a real-time basis. Power electronic inverters are necessary to facilitate utility-interactive V2G power injection control. Therefore, a VPL with a power electronic provision was assumed in this work. The real power P_o injected or absorbed from the grid, and reactive power Q_o injected to the grid, through inductive element X_L may be expressed as

$$\boxed{P_o = \frac{|EV|}{X_L}\text{Sin}(\delta) \quad | \quad Q_o = \frac{|EV|\cos(\delta) - E^2}{X_L}} \quad (2)$$

where δ is the power angle between the inverter bridge voltage V and the distribution network voltage E. From (2), δ is normally controlled to regulate P_o, while V is controlled to regulate Q_o. In Section III, modeling of the system parameters to be monitored is presented.

III. Modeling Parameters for Monitoring

In this section, the parameters for real-time monitoring of the power system are presented. An algorithmic paradigm was used to manage the system operations by real-time monitoring of the identified parameters, namely, power loss, energy loss, voltage stability, step voltage regulator (SVR) operations, and economic analysis.

1) Power Loss Computation: Fig. 1 depicts a feeder line segment with n number of V2G parking lot facilities. The per unit optimal power loss reduction, $\Delta P_{\text{LS\_V2G\_opt}}$, for a single VPL is defined as [12]

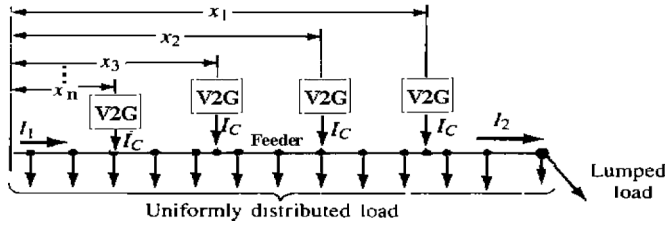

Fig. 1. n-V2G parking lot feeder system.

$$\Delta P_{\text{LS\_V2G\_opt}} = 3c\alpha x_1\left[(2 - x_1) + \lambda x_1 - c\right] \quad (3)$$

where the quantity x_i represents the position of the ith V2G parking lot, while the load pattern λ defines the loading characteristic of the line segment ($\lambda = 0$ represents uniformly distributed load, while $\lambda = 1$ represents lumped loads). Hence, the range, $0 < \lambda < 1$, defines the bounds of possible load pattern [12]. From (3), the following parameters are defined [12]:

$c = I_c(I_1)^{-1}$	$\lambda = I_2(I_1)^{-1}$	$\alpha = (1 + \lambda + \lambda^2)^{-1}$

Equation (3) indicates that power loss reduction in the network (due to V2G injecting reactive power) is a function of V2G location (x_1), sizing (c), and load pattern λ. The quantities, I_c, I_1, and I_2, are, respectively, the injected reactive current (from VPL), the reactive current at beginning, and at the end of the of feeder line segment. The parameters of (3) are obtained online for real-time computation of the power loss. The per unit energy loss reduction is discussed next.

2) Energy Loss Computation: The per unit optimal energy loss reduction, $\Delta\text{EL}_{\text{opt\_V2G}}$, in a three-phase distribution line segment is defined as (for $n = 1$) [12]

$$\Delta\text{EL}_{\text{opt\_V2G}} = \frac{3\alpha c}{1 - \lambda}\left[F_{\text{LD}} - c + \frac{c^2}{4F_{\text{LD}}}\right]T \quad (4)$$

where F_{LD} is the reactive load factor ($F_{\text{LD}} = Q/S$), and T is the normalized total period of time that the V2G parking lot is supplying reactive power. The model for the impact of V2G on voltage stability is presented next.

3) Voltage Stability Computation: The voltage stability index (VSI) formulation utilized in this research was the method described in [13]. Considering Fig. 2, the VSI for node m (VSI_m) is computed as [14]

$$\text{VSI}_m = \left(2\frac{V_m}{V_k}\cos(\delta_k - \delta_m) - 1\right)^2 \quad (5)$$

where V_m is the node voltage at node m and V_k is the node voltage at node k; δ_k is the voltage angle at node k, while δ_m is the voltage angle at node m. For a balanced system, the magnitude of VSI varies between unity (at no load) and zero (at voltage collapse). The voltage stability margin (VSM) of such a feeder depicted in Fig. 2 is given by [13], [14]

$$\text{VSM}_{k,m} = \prod_{i \in \Omega} \text{VSI} \quad (6)$$

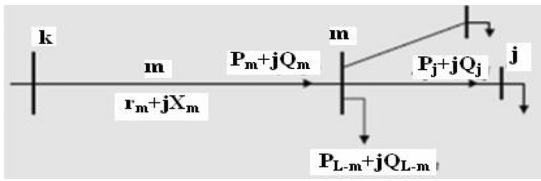

Fig. 2. Typical Radial Distribution System [14].

where Ω is a set of branches constituting the enter length of each feeder, starting from the source bus to the receiving end bus. A feeder with the lowest value of VSM is considered as the weakest feeder of the system, and is defined as [13]

$$\mathrm{VSM}_{\mathrm{sys}} = \min(\mathrm{VSM}_1, \mathrm{VSM}_2, \ldots, \mathrm{VSM}_j) \tag{7}$$

where j is the number of feeders in the system. The system VSM ($\mathrm{VSM}_{\mathrm{sys}}$) is an indicator of the nearness of the system to voltage collapse. Equations (5)–(7) provide an algorithmic basis for the real-time computation of the system's voltage stability.

4) Economic Analysis:

a) Economic Benefit Due to Released Generation Capacity: One of the considerations in real-time system management is the economic operation of the system. It is appropriate to monitor the hourly economic incentive $\Delta\$_G$ due to the released generation capacity ΔS_G when VPL is installed. The released generation capacity ΔS_G may be defined as

$$\Delta\$_G = 1 - \sqrt{\frac{C_2^2 + (1 - C_1)^2}{1 + C_2^2}} \times S_1 \times pf \times C_G \times Av \tag{8}$$

where pf is power factor, C_G is the cost of generation [to be provided by the Independent System Operators (ISO)], and Av is the availability of V2G vehicle per day (taken as 96% [5]). Also, S_1 is the complex power flowing from the "source" of a typical feeder line. From (12), the following are defined:

$$\boxed{C_1 = Q_c(Q_1)^{-1}(\mathrm{p.u.}) \quad | \quad C_2 = P(Q_1)^{-1}(\mathrm{p.u.})} \tag{9}$$

where Q_c and Q_1 are the reactive power injection from VPL and load reactive power demand, while P is real power flow in the feeder line. Note that $C_1 = 0$ represents no reactive power injection from the V2G parking lot, while $C_1 = 1$ represents reactive power injection equal to the load reactive power demand. Furthermore, $C_2 = 0$ represents no real power injection. Because of high kW demand in distribution networks, situations may arise when $C_2 > 1.0$. Economic incentives due to reduced energy losses are discussed next.

b) Economic Benefit Due Conserved Power: Conserved power loss ΔP represents the amount of kW power gained due to the penetration of V2G, and is defined as

$$\Delta P_i = P_{\mathrm{Loss},0} - P_{\mathrm{Loss},_i} \tag{10}$$

where ΔP_i and $P_{\mathrm{Loss,i}}$, respectively, represent the$i$th conserved power and power loss corresponding to the ith case or ith scenario; $P_{\mathrm{Loss},0}$ is the reference power loss for the original system that does not have V2G installation. The hourly dollar incentive $\Delta\mathrm{CP}_h$ due to conserved power is given by

$$\Delta\$\mathrm{CP}_h = Av \cdot \Delta P_i \times C_E. \tag{11}$$

5) Modeling SVR for Unbalanced Radial Network: The regulation of voltages in a distribution feeder is a significant concern for the electric utility because responsibility issues arise when customer's equipment is damaged due to either high or low voltages. Hence, providing statutory voltage levels at customer terminals is an integral part of quality of service, and can be monitored in real-time. The regulation of voltages in a distribution feeder can be achieved by using SVRs, load tap-changing transformers (LTC), and shunt capacitors. Only SVR shall be modeled in this paper because of its fast and efficient operation metrics.

SVR are auto-transformers, that regulates voltages in the range of $\pm 10\%$ with 32 steps divided into 16 steps up and 16 steps down, 5/8% change per step or 0.75-V change per step, on a 120-V base [17]. Taking V_L, V_s, and I_L, I_s as the voltage and current quantities at the load end and source end of SVR, respectively, and then the SVR may be modeled as [11]

$$\boxed{V_L = \frac{1}{a_R} V_s \quad | \quad I_s = \frac{1}{a_R} I_L \quad | \quad a_R = 1 \mp \frac{N_2}{N_1}} \tag{12}$$

where a_R is the regulator ratio, and N_2 and N_1 are, respectively, the secondary and primary turns ratio. The *minus sign* is used when the regulator is in the raise position and *plus sign* when in the lower position. For three-phase SVR models, a generalized matrix equation is defined such that [17]

$$\begin{bmatrix} V_s^{abc} \\ I_s^{abc} \end{bmatrix} = \begin{bmatrix} a' & b' \\ c' & d' \end{bmatrix} \cdot \begin{bmatrix} V_L^{abc} \\ I_L^{abc} \end{bmatrix} \tag{13}$$

where V_s^{abc}, V_L^{abc}, I_s^{abc}, and I_L^{abc} are the voltage and current three-phase quantities (a, b, c) at the source (s), and at the load (L), respectively. The $a'\,b'\,c'\,d'$ parameters in the above equation are 3×3 matrices. For a three-phase wye-connected SVR, the three-phase $a'\,b'\,c'\,d'$ parameters are [17]

$$\left.\begin{aligned} a' &= \begin{bmatrix} a'_{R\_a} & 0 & 0 \\ 0 & a'_{R\_b} & 0 \\ 0 & 0 & a'_{R\_c} \end{bmatrix} \quad b' = \begin{bmatrix} 0 & 0 & 0 \\ 0 & 0 & 0 \\ 0 & 0 & 0 \end{bmatrix} \\ c' &= \begin{bmatrix} 0 & 0 & 0 \\ 0 & 0 & 0 \\ 0 & 0 & 0 \end{bmatrix} \quad d' = \begin{bmatrix} \frac{1}{a'_{R\_a}} & 0 & 0 \\ 0 & \frac{1}{a'_{R\_b}} & 0 \\ 0 & 0 & \frac{1}{a'_{R\_c}} \end{bmatrix} \end{aligned}\right\} \tag{14}$$

where a'_{R-a}, a'_{R-b}, and a'_{R-c} are the effective turns ratios for phase a, b, c. It should be noted that the $a'\,b'\,c'\,d'$ parameters may also represent two-phase and one-phase components by filling the unused rows and columns with zeros.

Having modeled the indices to be monitored during system operation, the real-time algorithm to ensure the efficient system management using the indices is presented next.

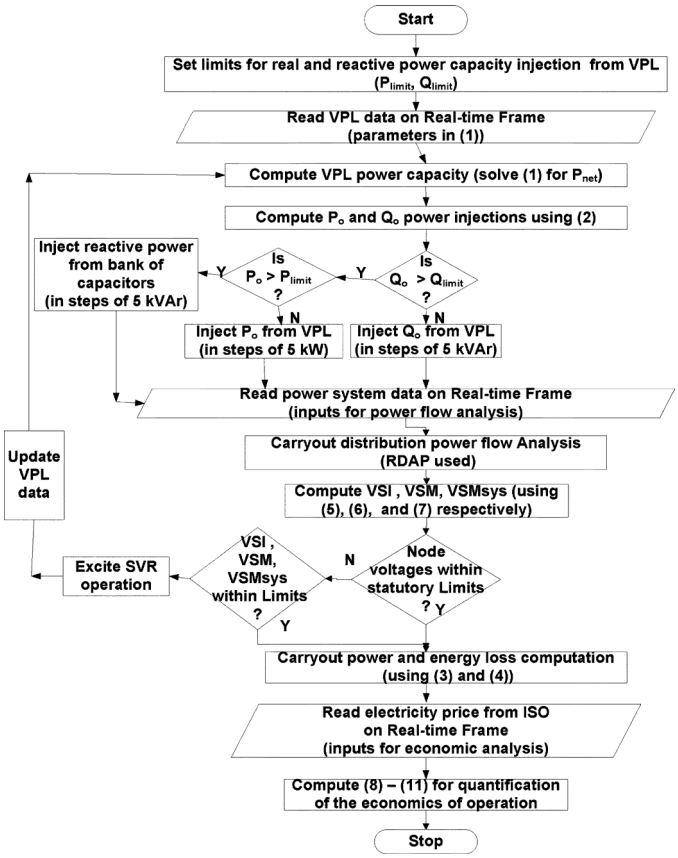

Fig. 3. Flowchart for real-time management of power systems with V2G.

IV. Real-Time Management Algorithm

In this section, the development and application of a real time monitoring diagnostic formulation of the power system is presented. The proposed algorithm is as presented in Fig. 3. To explain how the flowchart works, it is assumed that automation and control systems are installed at all the power system levels (from substation through ISO to the load center). This is necessary for real-time data acquisition. The real and reactive power threshold limits $(P_{\rm limit}, Q_{\rm limit})$ are set *ab initio* by initializing to $P_{\rm limit}$ and $Q_{\rm limit}$, respectively. Next, with the aid of supervisory control and data acquisition (SCADA), global positioning systems, and other intelligent electronic devices (IEDs), it is possible to capture the VPL data necessary for the computation of the instantaneous snapshot of the VPL power capacity. The VPL power capacity is computed using (1). Similarly, SCADA and IEDs are used to acquire the power system parameters $(\delta, V, E,$ and $X_L)$ required to compute P_o and Q_o using (2). Hence, as seen, the instantaneous snapshot of the VPL power capacity and the power system performance indices for real-time monitoring applications is established. It is important to note in the flowchart that the initialized quantities, $P_{\rm limit}$ and $Q_{\rm limit}$, are necessary to determine whether a capacitor may be required for supplementary reactive power injection (i.e., if the VPL real and reactive power limits are reached). Then, the operation of the system with V2G is simulated by solving the power flow and the VPL capacity at user selected time intervals. As the time progresses, the number of vehicles in a VPL may change. A power flow algorithm was necessary to compute the steady-state evaluation of the power system employing the acquired system data in order to determine the system performance using voltage stability quantification—VSI, VSM, and $\rm VSM_{sys}$ [computed from (5), (6), and (7)]. It should be noted that the power flow computation yields the parameters necessary for voltage stability evaluation, namely V_m, V_k, δ_k, and δ_m. If the voltage stability quantities are not within statutory limits, then the operation of SVR is activated (to adjust the bus voltages accordingly), before recomputing the VPL power capacity (after updating the VPL data to take care of possible entrance of a new V2G in the VPL after the previous iteration). This process continues till VSI, VSM, and $\rm VSM_{sys}$ are within the statutory limits for proper and optimal system operation.

An important issue in the management of the electric distribution network is the real-time coordination of SVR operations. This is because the dynamics of the SVR tap positions (due to the variability of V2G charging/discharging operations and load fluctuations) result in the wearing of the SVR over time, hence creating maintenance issues.

Therefore, the online operation of the SVR in real-time for optimal voltage control is discussed and presented in this paper. On this background, real-time monitoring diagnostic and management paradigm proposed in Fig. 3 is structured to monitor and control the SVR devices in such a way as to make the least possible tap-position changes. This can be achieved by other voltage remedial actions (like capacitor operation, and injection of real and reactive power) preceding the operation of the SVR. Also, proper knowledge of the power and energy loss in the system is necessary—hence, the flowchart shows power and energy loss computation [computed using (3) and (4)]. Finally, economic operation of the system is evaluated using (8)–(11). The importance of this study is highlighted in the real-time requirements of a smart grid, where economic and optimized operations are critical.

In this work, V2G penetration is defined as the percentage of the substation electric power capacity. For instance, 50% penetration in a system with 5-MW substation capacity means a cumulative V2G capacity of 2500 kW. The impact of one-phase and three-phase V2G interconnection at given penetration level was investigated with respect to impacts on three phases of the system. Seven case studies presented in Table I were used to investigate the impacts that different V2G penetration levels may have on the power system parameters to be monitored (voltage, voltage stability, SVR control, and power/energy loss). In Table I, V2G are either charging or discharging. When discharging, either kW or kVAr is injected to the feeder (hence VPL behaves like a power source) but consumes only kW when charging (load source). All appearances of "Case 1" in the results presented are merely to establish a quick comparison between the base case (Case 1) and other cases. In order to exhaustively explore possible system operational cases in a real-life scenario, a comprehensive study of the different penetration levels of V2G was performed with respect to the scenarios presented in Table II. Each scenario was further investigated in the context of the case studies.

In Section V, results and analysis are presented in the context of the above categories for the IEEE 13 test feeder.

TABLE I
CASE STUDIES (*50%≡ 2500 kW OR 2500 kVAr)

Case	% V2G Penetration		Comment
	Discharging Mode	Charging mode	
1.	0	0	Original System (Base Case)
2.	0	*50	All V2G consuming only kW
3.	50	0	All V2G injecting kW
4.	50	50	50% of V2G injecting kW, 50% Consuming kW
5.	50	50	50% of the V2G injecting KVAr, 50% Consuming kW
6.	50	0	All V2G injecting KVAr
7.	50/50	0	50% of V2G injecting KVAr and other 50% injecting kW

TABLE II
SCENARIO STUDIES (*50% ≡ 2500 kW OR 2500 kVAr)

Scenario	Activities
1	V2G injecting kVAr/kW or demanding kW on Phase A
2	V2G consuming 2500 kW on entire system at all load buses
3	V2G injecting 2500 kW to entire system at all load buses
4	V2G consuming 2500 kW and injecting 2500 kVAr in entire system
5	V2G injecting 2500 kVAr to entire system at load buses
6	V2G simultaneously injecting 2500 kW and 2500 kVAr to entire system

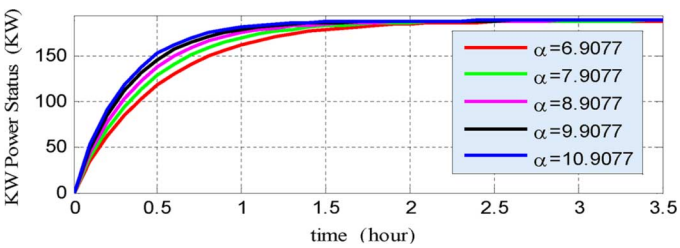

Fig. 4. Power demand of a V2G to be fully charged for any α.

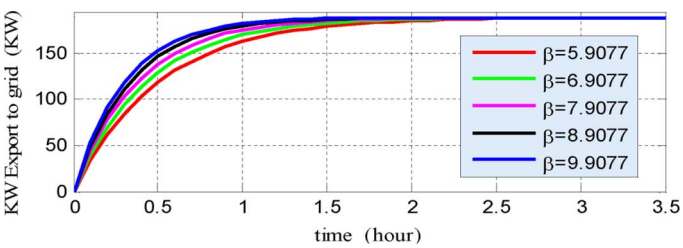

Fig. 5. Active power export to grid from a V2G vehicle.

V. NUMERICAL RESULTS

The results are presented in four sections, namely: 1) VPL electric power capacity, 2) IEEE 13 node test feeder as case studies, 3) generic study on power and energy loss, and 4) economic management of system with V2G.

A. VPL Electric Power Capacity

The VPL model in (1) was tested using the battery parameters for a Tesla Roadstars electric vehicle: $t_{\max} = 3.5$ h, $P_{\max} = 189$ kW [4]. However, before investigating VPL power capabilities, it is crucial to study the battery behavior of a single V2G in the VPL during charging and discharging operation. The power demand and power supply characteristic of a single V2G are as shown in Figs. 4 and 5. In computing power demand for a single V2G, for example, initial power in battery $P_{\text{EVo}} = 0$ kW, $n_d = 1$, and all power supply parameters in (1) were set to zero

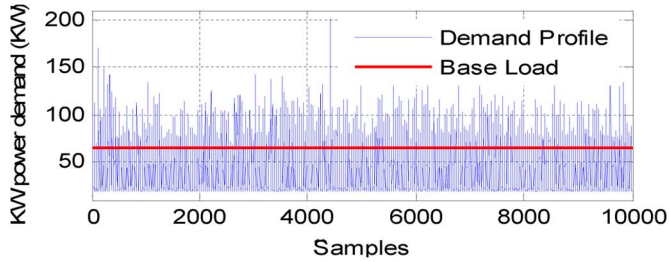

Fig. 6. Base load for 10-EV System of 10 000 samples.

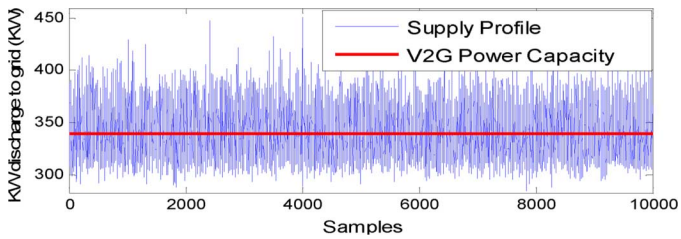

Fig. 7. Power capacity for 10-V2G system (10 000 samples).

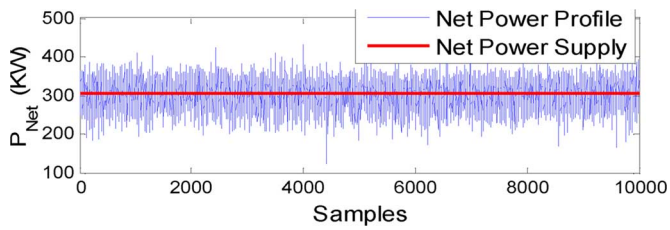

Fig. 8. Net power capacity for 10-V2G system (10 000 samples).

(i.e., β, t_{si}, n_s), and vice versa. The results show that both power demand profile for every α (Fig. 4) and power supplied to the grid for every β (Fig. 5) increase as service time increases. Extending the study to a VPL of 10-V2G capacity, a stochastic approach was used to ascertain the effective VPL power capabilities (for 10 000 samples) [4]. The results are presented in Fig. 6–8. The results show that the net power demand is 66 KW (Fig. 6, all V2G charging batteries), net power discharged to grid is 342 KW (Fig. 7, all V2G supplying power to grid), and net power supply to grid is 276 kW (Fig. 8, some V2G charging, and others discharging power to grid). The net power was the power injection at any given PQ bus for power flow analysis.

B. IEEE Test Systems as Case Study

The IEEE 13 node test feeder data used in this study were presented in [15]. The impact of different penetration levels of V2G on the system parameters was investigated. In order to clearly see the effect of the V2G on the test feeders, the voltage regulators and shunt capacitors in the system were first disabled (because these devices also affect system parameters to be monitored). The seven cases in Table I and the six scenarios in Table II were then applied.

The six scenarios in Table II may be grouped into two categories, namely, Category A (scenario 1) and Category B (scenarios 2–6). Category A considers impact of one-phase V2G integration, while Category B considers system-wide V2G integration. These categories are presented next.

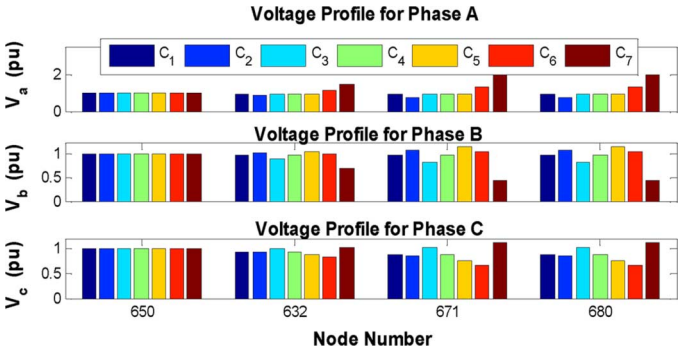

Fig. 9. Voltage profile for main feeder of IEEE 13 node test feeder for V2G interconnection at Phase A (V_a, V_b, V_c, are phase a, b, c voltages).

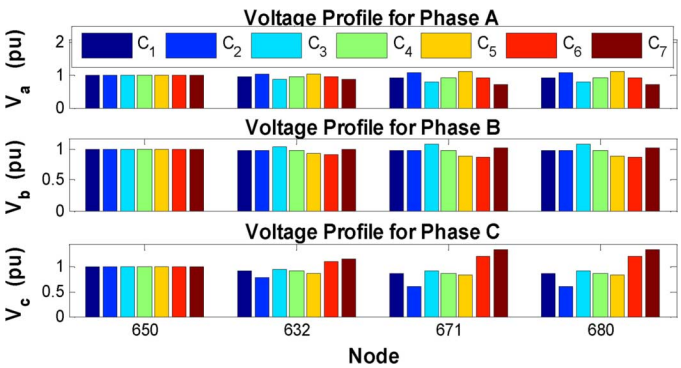

Fig. 10. Voltage profile at main feeder for three-phase V2G interconnection of IEEE 13 test feeder (V_a, V_b, V_c, are phase a, b, c voltages).

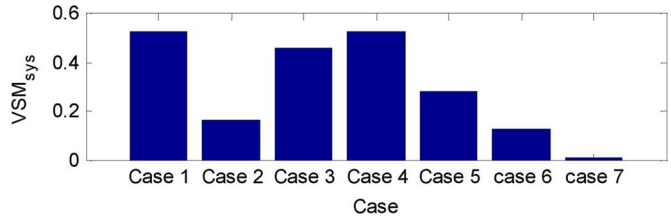

Fig. 11. VSM_{sys} for V2G interconnection at Phase A of IEEE 13 test feeder.

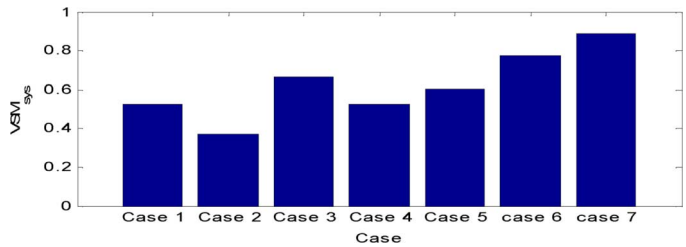

Fig. 12. VSM_{sys} for three-phase V2G interconnection of IEEE 13 test feeder.

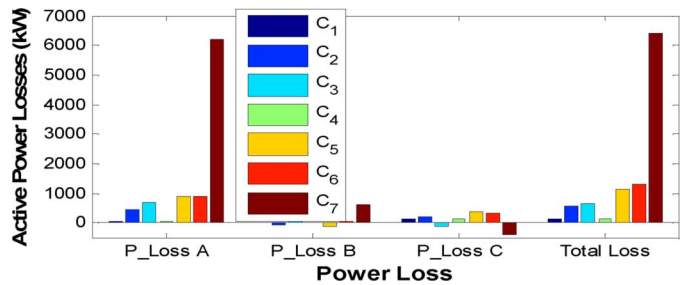

Fig. 13. Kilowatt (kW) power losses for V2G facility at Phase A of IEEE 13 test feeder.

1) Category A: Scenario 1: As seen from Section IV, scenario 1 is a phase A V2G operation. The IEEE 13 node test feeder data shows that N_652 is a phase_A lateral. However, it is necessary to compare system performance for one-phase integration with three-phase V2G integration. Node 675 is three-phase node [15]. The effect of the one-phase and three-phase integrations on the system parameters is studied.

a) Voltage Profile: The results of the voltage profile for one-phase interconnection are presented in Fig. 9 (where C_i represents an ith case, such as defined Table I). The results show that interconnecting V2G facility at Phase A altered the voltage profile of the entire system for all the seven cases (only main feeder nodes considered). On the other hand, three-phase operation (presented in Fig. 10) resulted in a more stable voltage profile, thereby revealing the merits of installing three-phase VPL facilities over the one-phase integration.

Other one-phase studies in scenarios 2 and 3 (not presented) revealed similar results as in scenario 1. Therefore, it can be seen that because of unbalanced loading and resulting unbalanced line currents in one-phase integrations, the voltage profile becomes more adversely affected than in three-phase integration.

b) Voltage Stability: The voltage stability margin, VSM_{sys}, was computed using (5)–(7). The results presented in Fig. 11 show that for one-phase integration, significant VSM_{sys} occurred at Case 4. However, for three-phase integration (results presented in Fig. 12), significant VSM_{sys} occurred at Cases 3, 5, 6, and 7 (with higher magnitudes). It was further observed that the improved system VSM took place at the feeder where power was injected into the distribution system, with the highest impact made in Case 7. The contrast occurred in Case 2, where all the V2G in the system were operated in demand mode. This further shows that three-phase operation resulted in improved system security over one-phase integration.

c) Power Loss: The power loss computation of the system from power flow analysis (using RDAP) shows that excessive power loss occurred in one-phase (Fig. 13) rather than in three-phase (Fig. 14). Three-phase V2G integration resulted in reduced power loss (with respect to Case 1) by 69.6% when operated in Case 7, 58.8% when operated in Case 3, and 19% when operated in Case 6.

d) SVR Operation: In all the analyses done so far in this research, the incorporation of SVR was ignored so that the impact of V2G on the system would be established. However, it is crucial to investigate how the penetration of V2G will affect the SVR operation, as this is related to maintenance issues for the SVR device. The SVR was installed at node 650 of the IEEE 13 node feeder. V2G is expected to affect the voltage profile of the feeder network. Using (12)–(14), the SVR tap positions per phase for the different case studies were computed for one-phase Phase A integration, and the result is shown in Fig. 15. Negative tap position may arise as can be seen in Fig. 16 (because SVR has 32 steps, defined by $-16 \leq T_p \leq 16$) [11].

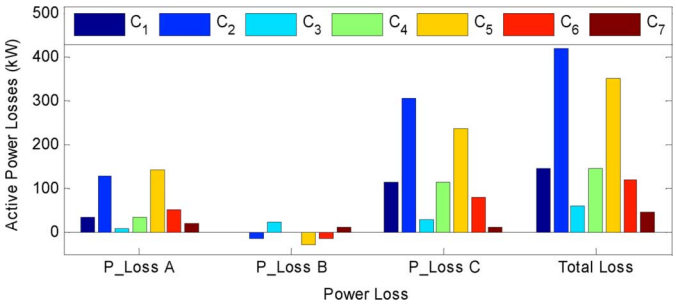

Fig. 14. Kilowatt (kW) power loss for three-phase V2G interconnection of IEEE 13 Feeder.

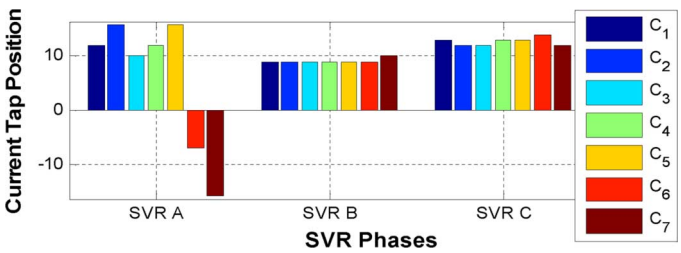

Fig. 15. SVR tap positions for V2G interconnection at Phase A.

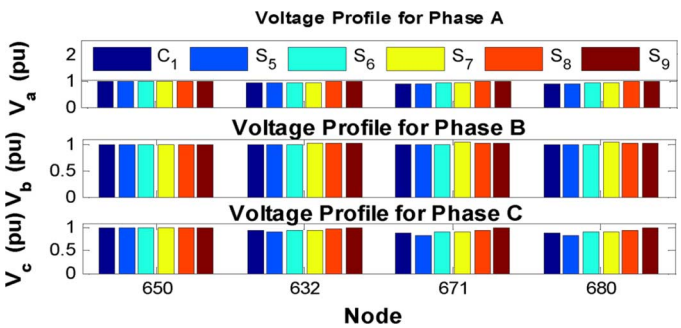

Fig. 16. Voltage profile at main feeder for Category B V2G interconnection.

The dynamics of the SVR motor system depends on the deviation of the node voltage at the load center from the nominal voltage setting of the SVR. For lower voltage profiles, the SVR tap-changing mechanism will move up in order to raise the voltage to a safe and acceptable limit. This explains why the Phase A SVR tap of position of SVR moved from 12 to 16 for Cases 2 and 5 in Fig. 15. The V2G facility loading extra 2500 kW on Phase A (Case 2) of the distribution network will definitely result in high current flow through the SVR_A, hence resulting in the increased tap position. A look at Case 3 of Phase A shows that the tap position went down from 12 to 10, thereby alluding to increased voltage rise in Phase A when 2500 kW was injected at node 652 (Fig. 15). In Cases 6 and 7, the tap positions, respectively, went from 10 to -7 and 10 to -16, respectively, because of the higher voltage levels. Because Phase B was lightly loaded, the tap position is at position 9. However, the SVR tap position is steady in Phase B because the voltage variation was not significant at Phase B of the load center. Hence, unbalances between phases make the SVR to set different tap positions for each phase (and, therefore, creates reduced reliability of the device over time of operation due to unbalanced loading).

Fig. 17. System VSM for Category B V2G interconnection of IEEE 13 Feeder.

2) Category B: Scenarios 2, 3, 4, 5, and 6: It is expedient, however, to investigate how a widespread use of the V2G facilities in the entire system affects the distribution system performance. This consideration will mimic the real-life situation where a mix of three-phase, two-phase, and one-phase V2G facilities may be installed at many different parts of the distribution system.

a) Voltage Profile: The voltage profile of the IEEE 13 node test feeder when V2G was operated with respect to the set of scenarios defined in Category B is presented in Fig. 16. The designations S_i represent ith scenario. The results in Fig. 16 show a more stable voltage profile than the voltage profile in three-phase single spot integration (Fig. 10), and better off than one-phase voltage profile (Fig. 9).

This suggests that the entire system in Category B operation is, more or less, in the neighborhood of balance than Category A. This result could be a motivation for power system operators to take advantage of installing V2G in many parts of the radial feeder system.

b) Voltage Stability: The voltage stability for Category B is presented in Fig. 17. From the figure, it is discovered that the highest VSM magnitude occurred at Case 6. This is because of the cumulative effect of injecting both kW and kVAr. A comparison of VSM between different cases and scenarios (not shown) indicates that Category B offers better system security than Category A and V2G three-phase spot integration.

c) Power Loss: The kW power losses for Category B V2G interconnection are presented in Fig. 18. Results show that three-phase and system-wide V2G integrations in the distribution network resulted in improved power losses over one-phase integrations. This was because the entire system is in a more balanced state in Category B than in Category A. Therefore, power system operators may operate in Category B for more efficient operation. From this study, it is clear that the system performance depends on the manner of system of operation.

d) SVR Operations: The results of SVR tap positions for Category B operation are presented in Fig. 19. A comparison of Figs. 19 and 15 shows that fewer tap-changes took place in Category B than Category A (all positive tap changes). This suggests that system-wide integration of V2G would result in less activation of the SVR motor (hence less maintenance requirement) than the Category A option. The real-time power systems management proposed in Fig. 3 will ensure that this critical objective is achieved.

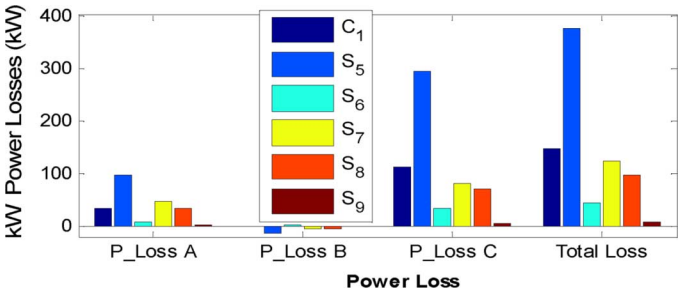

Fig. 18. Kilowatt (kW) loss for Category B V2G interconnection of IEEE 13 Feeder.

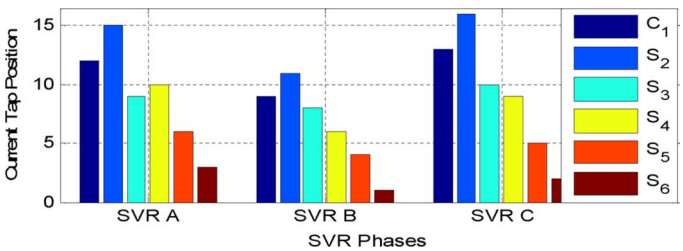

Fig. 19. SVR tap positions for Category B operation.

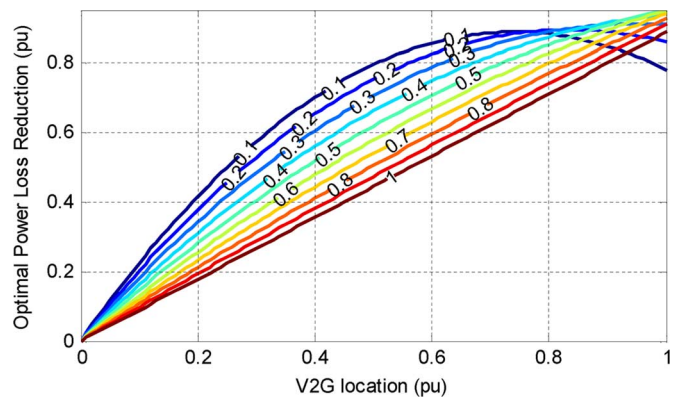

Fig. 20. Kilowatt (kW) loss reduction due to optimum-sized VPL for various λ.

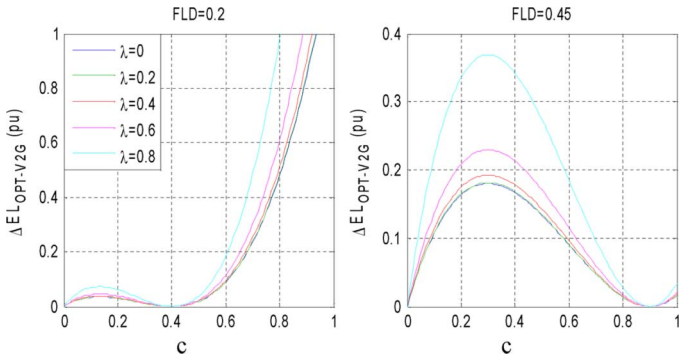

Fig. 21. Optimal energy loss with any V2G reactive compensation ratio and various load pattern for a V2G facility at optimum site ($F_{\rm LD} = 0.2$ to 0.45 p.u.).

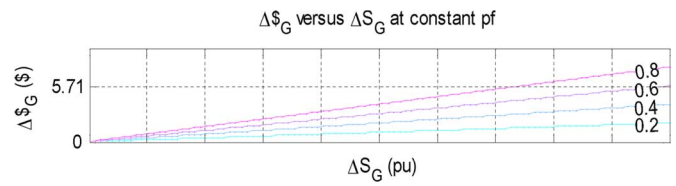

Fig. 22. Dollar incentives with respect to ΔS_G at constant *pf*.

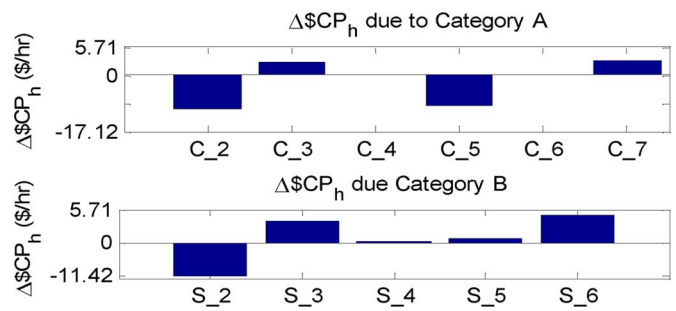

Fig. 23. Dollar incentive due to conserved power for Categories A and B.

C. Generic Study on Power and Energy Loss

The study made in section B only deals with the impact of VPL at a specific location on the network. It is, however, necessary to investigate how the V2G location and load pattern can impact the system power loss. Using (3), the power loss reduction was computed and results are presented in Fig. 20. The results show that power loss reduction increases with increasing VPL location, although a limit may exist. The result also further shows that increasing λ (contours) leads to improved loss reduction. Hence, from Fig. 20, the least peak power loss reduction is about 89%, when $\lambda = 0.1$ and $x_1 = 0.75$ p.u. (i.e., 89% power loss reduction can be achieved when VPL is optimally located at 0.75 p.u.). Moreover, the result shows that as $\lambda \rightarrow 1$, the characteristic tends towards linearity.

Energy loss was computed using (4), and results presented in Fig. 21, indicate that as $\lambda \rightarrow 1$, the optimum energy loss reduction increases. Moreover, the energy loss reduction increases as FLD increases.

It is evident from this result that for all values of λ, when reactive load factors are 0.2 and 0.45, the use of VPL injecting reactive power with corrective ratios of 0.4 and 0.9, respectively, results in a zero energy loss reduction. It is a critical operational consideration for system planners to know *a priori* the level of injection that will result in zero energy loss condition. From Figs. 20 and 21, it could be observed that a 95% loss reduction is possible.

D. Economic Management of the System With V2G

Using (8) and (9), and fixing S_1, and pf, respectively as 0.1 MVA, 0.8, the values of economic incentives due to released generation capacity are computed and results presented in Fig. 22. The result show that economic incentives increase as ΔS_G, increases. Using (11), the dollar incentive due to conserved power is presented in Fig. 23, for Category A and Category B operations. The results show that operating in Cases 2 and 5 resulted in economic loss, while operating in Cases 3 and 7 and Scenarios 3, 5, and 6 resulted in economic incentives. A critical look at Fig. 23 shows that economic losses were incurred in operations where VPLs were consuming kW load (demanding power from grid, when battery is charged), while significant economic incentives are supported by operations where V2G parking lots are exporting either kW power, or both kW and kVAr (discharging power to grid). The insignificant economic

gain in Scenario 5 shows that injecting only kVAr into the distribution network can promise economic incentive if the optimal amount of kVAr is injected. Furthermore, Case 4 and Scenario 4 operations resulted in no loss/gain in economic incentive. This is because Case 4 and Scenario 4 operations have the same power loss magnitudes as Case 1 (i.e., the original system)—thereby resulting in null differential economic loss when (10) and (11) are applied.

VI. Conclusion

This paper proposed an algorithmic procedure for a real-time operation of the power system with V2G penetration. The potentials of a VPL were first explored. The results show that a 10-V2G capacity VPL can promise net power demand of 66 KW, and a net power supply to grid of amount 276 kW. The paper also explored the impact of VPL on the power system operational health. The indices identified for measurement of the power system operational state are voltage profile, voltage stability, SVR operation, power loss, and energy loss. Mathematical models were used to study how different operational scenarios of VPL may affect the system operational health. An economic study was also made to investigate operations that may justify economic operation. IEEE 13 node test feeder was used as a case study. Results using the test feeder showed that three-phase and system-wide V2G integrations resulted in improved system operational health, and yielded more economic incentive than one-phase integrations. Results also showed that optimally locating VPL can promise 95% power and energy loss reduction (relative to a network without V2G). This paper may be helpful to system operators interested in real-time management of their networks.

References

[1] S. Khushalani, J. M. Solanki, and N. N. Schulz, "Development of 3-phase unbalanced power flow using PV and PQ models for DG and study of the impact of DG models," *IEEE Trans. Power Syst.*, vol. 22, no. 3, pp. 1019–1025, Aug. 2007.

[2] S. Deilami, A. S. Masoum, P. S. Moses, and M. A. S. Masoum, "Real-time coordination of plug-in electric vehicle charging in smart grids to minimize power losses and improve voltage profile," *IEEE Trans. Smart Grid*, vol. 2, no. 3, pp. 456–467, Sep. 2011.

[3] August 14, 2003 Blackout NERC Final Report, Jul. 13, 2004, pp. 1–5.

[4] U. C. Chukwu and S. M. Mahajan, "V2G electric power capacity estimation and ancillary service market," in *Proc. IEEE PES GM*, 2011, pp. 1–8.

[5] W. Kempton and J. Tomic, "Vehicle-to-grid power fundamentals: Calculating capacity and net revenue," *J. Power Sources*, vol. 144, no. 1, pp. 268–279, 2005.

[6] J. Tomí and W. Kempton, "Using fleets of electric-drive vehicles for grid support," *Energy Policy*, vol. 36, pp. 3578–3587, 2008.

[7] W. Kempton and J. Tomic, "Vehicle to grid implementation: From stabilizing the grid to supporting large-scale renewable energy," *J. Power Sources*, vol. 144, no. 1, pp. 280–294, 2005.

[8] W. Kempton and S. E. Letendre, "Electric vehicles as a new source for electric utilities," *Trans. Res. Part D*, vol. 2, no. 3, pp. 157–175, 1997.

[9] S. Letendre and W. Kempton, "The V2G concept: A new model for power?," *Public Utilities Fortnightly*, pp. 17–26, 2002.

[10] D. Yu, Z. Xiaohu, B. Sanzhong, S. Lukic, and A. Huang, "Review of non-isolated bi-directional DC-DC converters for PHEV charge station application at municipal parking decks," in *Proc. IEEE Applied Power Electronics Conf. and Expo. (APEC)*, 2010, pp. 1145–1151.

[11] A. Y. Saber and G. K. Venayagamoorthy, "Optimization of vehicle-to-grid scheduling in constrained parking lots," in *Proc. PES GM*, , 2009, pp. 1–8.

[12] T. Gonen, *Electric Power Distributed System Engineering*, 2nd ed. New York, NY, USA: McGraw-Hill, 1987, pp. 414–435.

[13] M. H. Haque, "A linear static voltage stability margin for radial distribution systems," in *Proc. IEEE PES GM*, Quebec, Canada, 2006, pp. 1–6.

[14] G. Mohan and P. Aravindhababu, "Load shedding algorithm for avoiding voltage instability in distribution systems," *Int. J. Electron. Eng.*, vol. 1, no. 1, pp. 39–45, 2009.

[15] IEEE 13 Node Test Feeder [Online]. Available: http://ewh.ieee.org/soc/pes/dsacom/testfeeders.html

[16] G. Garcia-Rodrigo and H. G. Vlachogiannis, "Letter to the editor: Electric vehicle demand model for load flow studies," *Elect. Power Compon. Syst.*, vol. 37, pp. 577–582, 2009.

[17] W. H. Kersting, *Distribution System Modeling and Analysis*, 2nd ed. Boca Raton, FL, USA: CRC Press, 2002, pp. 120–147.

Uwakwe Christian Chukwu (S'07) was born in Mburubu, Enugu State, Nigeria. He graduated from the Electrical and Electronic Engineering Department, Enugu State University of Science and Technology, Nigeria, with the B.Eng. degree in electrical and electronics engineering, in 1996. In 2003, he received the M.Tech. degree in electrical engineering from Rivers State University of Science and Technology, Nigeria. He received the Ph.D. degree (electrical) from Tennessee Technological University, USA, in 2011.

He was a lecturer with the University of Port Harcourt, Nigeria, from 2004 to 2008. Currently, he is a faculty member in the Department of Industrial and Electrical Engineering Technology, South Carolina State University. His research interests are power systems, smart grid, renewable energy and microgrids, and V2G and energy scavenging technologies.

Satish M. Mahajan (S'86–M'87–SM'09) was born in India and received the B.E. (electrical) degree from the University of Poona, in 1978. He received the M.S.E.E. degree from the State University of New York at Buffalo, in 1983, and the Ph.D. degree (electrical) from the University of South Carolina at Columbia, in 1987.

Since 1987, he has been on the faculty of the Electrical Engineering Department, Tennessee Technological University (TTU). His research interests are related to the physical phenomena of optoelectronic and H.V. devices, and modeling of conventional and renewable power systems.